Contrib Mineral Petrol (2004) 148: 55–68
DOI 10.1007/s00410-004-0583-1

ORIGINAL PAPER

C. McCammon · M. G. Kopylova

A redox profile of the Slave mantle and oxygen fugacity control in the cratonic mantle

Received: 4 December 2003 / Accepted: 19 April 2004 / Published online: 17 July 2004

Abstract The authors report a redox profile based on Mössbauer data of spinel and garnet to a depth of 210 km from mantle xenoliths of the northern (N) and southeastern (SE) Slave craton (northern Canada). The profile transects three depth facies of peridotites that form segments of different bulk composition, represented by spinel peridotite, spinel–garnet peridotite, low-temperature garnet peridotite, high-temperature garnet peridotite, and pyroxenite. The shallow, more depleted N Slave spinel peridotite records lower oxygen fugacities compared to the deeper, less depleted N Slave spinel–garnet peridotite, consistent with their different spinel Fe^{3+} concentrations. Garnet peridotites show a general reduction in $\Delta\log f\mathrm{O}_2$ (FMQ)s with depth, where values for garnet peridotites are lower than those for spinel–garnet peridotites. There is a strong correlation between depletion and oxygen fugacity in the spinel peridotite facies, but little correlation in the garnet peridotite facies. The strong decrease in $\Delta\log f\mathrm{O}_2$ (FMQ) with depth that arises from the smaller partial molar volume of Fe^{3+} in garnet, and the observation of distinct slopes of $\Delta\log f\mathrm{O}_2$ (FMQ) with depth for spinel peridotite compared to spinel–garnet peridotite strongly suggest that oxygen fugacity in the cratonic peridotitic mantle is intrinsically controlled by iron equilibria involving garnet and spinel.

C. McCammon (✉)
Bayerisches Geoinstitut, Universität Bayreuth, 95440 Bayreuth, Germany
E-mail: catherine.mccammon@uni-bayreuth.de
Tel.: +49-921-553709
Fax: +49-921-553769

M. G. Kopylova
Geological Sciences Division, Earth and Ocean Sciences, The University of British Columbia, 6339 Stores Road, Vancouver, Canada

Introduction

Efforts over the past 20 years have produced much data concerning upper mantle oxygen fugacity, and although agreement is not universal, a relatively consistent picture is emerging. The relative oxygen fugacity ($\Delta\log f\mathrm{O}_2$ [FMQ]) measured for lithospheric upper mantle is heterogeneous, where trends in oxygen fugacity have been noted to occur with metasomatism (e.g., McCammon et al. 2001), partial melting (e.g., Bryndzia and Wood 1990) and tectonic environment (e.g., Wood et al. 1990; Ballhaus 1993; Parkinson and Arculus 1999).

Calibration of an olivine-orthopyroxene-garnet oxybarometer (Gudmundsson and Wood 1995) has enabled oxygen fugacity determinations to be extended to much greater depths, in particular to 170 km beneath the Fennoscandian Shield (Woodland and Peltonen 1999) and to 220 km within the Kaapvaal craton (Woodland and Koch 2003). While a global picture is still lacking, the general pattern of relative oxygen fugacity ($\Delta\log f\mathrm{O}_2$ [FMQ]) decreasing with depth demonstrated by these studies supports earlier predictions of a reduced upper mantle within the garnet peridotite facies (Wood et al. 1990; Ballhaus and Frost 1994; Ballhaus 1995; Wood et al. 1996).

Studies of mantle xenoliths from the Slave craton have revealed a number of similarities with the Kaapvaal craton, but also a number of differences (Kopylova et al. 1999), including the identification of two segments in the upper part of the Slave mantle with different bulk compositions, representing different degrees of depletion from partial melting (Kopylova and Russell 2000; Kopylova and Caro 2004). A redox profile through the Slave cratonic mantle would therefore provide complementary data for constructing a more global picture of oxygen fugacity variation in the deeper part of the lithospheric mantle, and the opportunity for a more detailed examination of the relation between oxygen fugacity and the degree of depletion.

While the number of studies reporting oxygen fugacities for mantle rocks continues to grow, the nature

of what controls oxygen fugacity remains an open question. Canil et al. (1994) examined the relative buffering capacities of different equilibria (involving Fe, C, H or S) based on their estimated mantle abundance, and concluded that no single equilibrium could be considered to dominate overall. A more recent comparison of Fe_2O_3 and carbon abundance showed that concentrations vary depending on rock type, suggesting that the nature of buffering varies for different regions of the mantle (Luth 1999).

To address all of these issues, we have determined a redox profile for a 130-km-thick mantle segment in the Slave craton that transects three depth facies of peridotite and segments of different bulk compositions. We employed Mössbauer spectroscopy to measure Fe^{3+} concentrations in mantle garnet and spinel and calculated $\Delta\log f O_2$ (FMQ) from equilibria involving these accessory minerals. The data demonstrate a strong correlation between depletion and oxygen fugacity in the spinel peridotite facies, but little correlation in the garnet peridotite facies. In addition, our data suggest that iron equilibria have the prevailing capacity to buffer oxygen fugacity in the cratonic peridotitic mantle.

Sample description

Peridotitic mantle xenoliths were collected for this study from the drill core of the Jericho and the 5034 (Gahcho Kue cluster) kimberlite pipes. The kimberlites are located in the northern and southeastern parts of the Slave Craton (northern Canada, Fig. 1 in Kopylova and Caro 2004). The Jericho pipe was dated as Middle Jurassic (172 ± 2 Ma by Rb–Sr and U–Pb geochronology) and the 5034 kimberlite as Middle Cambrian (539 ± 2 Ma by the Rb–Sr method on phlogopite) (Heaman et al., in press). Both kimberlites are diamondiferous and host spectacular suites of fresh mantle xenoliths.

Five types of the Jericho mantle xenoliths (N Slave) were selected for the study: spinel peridotite, low-T spinel–garnet peridotite, low-T garnet peridotite, high-T garnet peridotite, and megacrystalline pyroxenites grading into crystalline intergrowths of megacrysts. The petrology of garnet-bearing rock types and their mineral analyses were reported in Kopylova et al. (1999), and their bulk compositions can be found in Kopylova and Russell (2000). Mineral analyses for the Jericho spinel peridotites that have not been previously published are listed in Table 1. The Gahcho Kue peridotites (SE Slave) are described in Kopylova and Caro (2004). For this study, we selected the peridotite that has coarse and deformed textures. Note, however, that deformed peridotite of the N Slave almost always shows temperatures higher than the conductive geotherm and is therefore classified as high-T peridotite, whereas deformed peridotite of the SE Slave shows temperatures that plot along the conductive geotherm and is therefore classified as low-T peridotite.

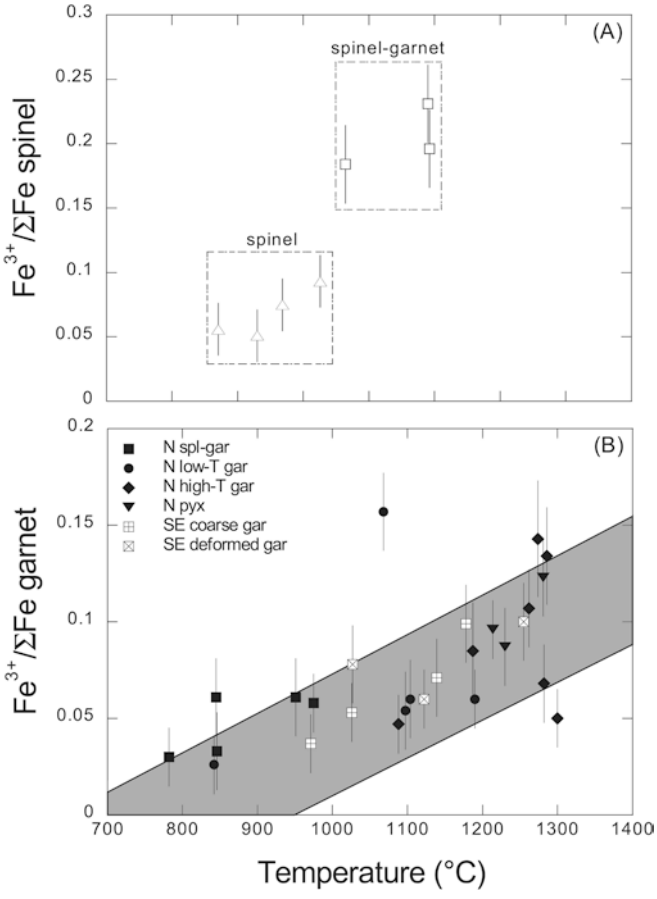

Fig. 1a, b Range of Fe^{3+}/Σ Fe in (**a**) spinel and (**b**) garnet in upper mantle xenoliths of the Slave craton. Equilibration temperatures for spinel are based on OW-geotherm estimates, while those for garnet are based on BK–AlBK estimates. Spinels show distinct values depending on rock type due to the depleted nature of spinel peridotite (different rock types are grouped by *dashed boxes*). Garnet values plot roughly along the literature trend (Woodland and Koch 2003 and references therein), which is indicated by the *shaded region*. Symbols are as follows: *open triangle* spinel in N Slave spinel peridotite, *open square* spinel in N Slave spinel–garnet peridotite, *solid square* garnet in N Slave spinel–garnet peridotite, *solid circle* N Slave low-T garnet peridotite, *solid diamond* N Slave high-T garnet peridotite, *solid triangle* N Slave pyroxenite and megacrysts, *square with plus* SE Slave coarse low-T garnet peridotite, *square with cross* SE Slave deformed low-T garnet peridotite

Experimental procedure

Garnet and spinel concentrates were prepared by hand picking under a binocular microscope. The garnet was treated with an acid wash of diluted HCl and HF, and in the case of strongly altered garnets, an additional wash of strong HF was used. Single grains of garnet and spinel were chosen from each monomineralic concentrate using a binocular microscope with selection criteria based on appearance (transparent and free of alteration), diameter and thickness. Grains were mounted between pieces of cellophane tape and masked with 25-μm-thick Ta foil drilled with a 500-μm hole.

Table 1 Mineral compositions of spinel-bearing peridotites from N Slave (Jericho pipe)

Rock type mineral (average)	10-12a low-T spinel–garnet lherzolite					11-18 spinel harzburgite			9-12 spinel harzburgite			44-12 spinel lherzolite				8-7 spinel lherzolite		
	Ol (5)	Opx (5)	Cpx (4)	Grt (5)	Spl (5)	Ol (4)	Opx (3)	Spl (4)	Spl (3)	Ol (3)	Opx (3)	Spl (11)	Ol (4)	Opx (3)	Cpx (5)	Spl (6)	Ol (2)	Opx (4)	Cpx (5)	Spl (7)
SiO_2	41.28	58.33	54.76	41.31	ND	41.36	57.91	ND	ND	41.68	58.48	ND	41.51	57.50	54.51	ND	41.40	57.69	54.71	ND
TiO_2	ND	ND	ND	0.03	0.08	ND	ND	0.02	0.04	ND	ND	0.02	ND	0.03	0.03	0.07	ND	ND	0.05	ND
Al_2O_3	ND	0.59	2.02	20.74	11.77	ND	1.36	25.77	22.45	ND	0.83	17.65	ND	1.85	2.16	27.62	ND	1.37	1.66	22.51
Cr_2O_3	ND	0.18	1.49	4.85	54.55	ND	0.36	44.91	47.73	0.02	0.21	52.83	0.02	0.51	1.01	41.99	0.04	0.37	0.68	47.68
FeO (tot)	7.45	4.76	1.73	8.69	22.17	6.75	4.50	14.96	15.79	6.78	4.31	16.60	6.88	4.49	1.20	15.37	6.61	4.20	1.02	15.40
MnO	0.09	0.11	0.05	0.57	0.08	0.10	0.13	0.08	0.08	0.07	0.11	0.09	0.07	0.10	0.06	0.09	0.09	0.07	0.04	0.08
MgO	51.27	36.56	16.39	18.49	10.71	52.08	36.36	14.21	13.32	51.78	36.67	12.38	51.78	36.06	17.06	14.30	51.83	34.95	17.35	13.47
CaO	ND	0.15	21.73	5.92	ND	ND	0.14	ND	ND	ND	0.14	ND	ND	0.19	22.87	ND	ND	0.21	23.64	ND
NiO	0.38	0.08	0.04	NA	0.07	0.37	0.05	0.06	0.04	0.41	0.07	0.06	0.38	0.06	0.03	0.05	0.43	ND	0.05	0.06
Na_2O	ND	ND	1.64	0.01	NA	NA	ND	NA	NA	ND	ND	NA	ND	0.03	1.05	NA	ND	0.08	0.76	NA
Total	100.50	100.80	99.85	100.61	99.46	100.71	100.82	100.03	99.47	100.75	100.86	99.63	100.66	100.83	100.00	99.52	100.43	98.96	99.98	99.23
Cr/(Cr + Al)					0.757			0.539	0.588			0.668				0.505				0.587

ND below minimum detection limits, *NA* not analysed, *Ol* olivine, *Opx* orthopyroxene, *Cpx* clinopyroxene, *Grt* garnet, *Spl* spinel

Dimensionless absorber thicknesses for garnet were generally between two and three (5–7 mg Fe/cm^2) and for spinel between four and six (10–15 mg Fe/cm^2).

Mössbauer spectra were recorded at room temperature (293 K) in transmission mode on a constant acceleration Mössbauer spectrometer using either a nominal 1.85-GBq ^{57}Co source in a 6-μm Rh matrix (conventional source) or a nominal 370-MBq ^{57}Co high specific activity source in a 12-μm Rh matrix (point source). The velocity scale was calibrated relative to 25 μm α-Fe foil using the positions certified for National Bureau of Standards (now called the National Institute of Standards and Technology) standard reference material no. 1541; line widths of 0.28 mm/s (conventional source) and 0.36 mm/s (point source) for the outer lines of α-Fe were obtained at room temperature. Further description of the method using a point source (Mössbauer milliprobe) is given in McCammon et al. (1991) and McCammon (1994).

Mössbauer spectra for garnet and spinel were fitted to Lorentzian and Voigt doublets depending on spectral resolution with either one (garnet) or two (spinel) doublets assigned to Fe^{2+} and one doublet assigned to Fe^{3+} according to current models in the literature (e.g., Amthauer et al. 1976; Li et al. 2002) using the commercially available fitting program NORMOS written by R.A. Brand (distributed by Wissenschaftliche Elektronik GmbH, Germany) and RECOIL written by K. Lagarec and D. Rancourt (distributed by Intelligent Scientific Applications Inc, Canada). Absorption due to Fe^{3+} was well resolved in all of the spectra, and values for $Fe^{3+}/\Sigma Fe$ were calculated based on relative area ratios corrected for thickness effects and differences in recoil-free fraction. The latter correction was based on the Debye model with assumed Mössbauer temperatures of 340 and 400 K for garnet Fe^{2+} and Fe^{3+}, and 330 and 400 K for spinel Fe^{2+} and Fe^{3+}, respectively (Amthauer et al. 1976; De Grave and Van Alboom 1991). The uncertainties given for the Mössbauer determination of Fe^{3+}/Σ Fe are based on errors from the fit to the given model, and uncertainties in the model itself.

Results and calculation of oxygen fugacity

Results for $Fe^{3+}/\Sigma Fe$ in garnet and spinel are presented in Tables 2 and 3. Calculations of $Fe^{3+}/\Sigma Fe$ from the electron microprobe data based on stoichiometry deviated significantly from these data; hence only Mossbauer determinations of $Fe^{3+}/\Sigma Fe$ were used in the present work.

Variations of $Fe^{3+}/\Sigma Fe$ in spinel and garnet reveal several patterns. Fe^{3+} concentrations in spinel show a striking contrast between spinel and spinel–garnet peridotite (Fig. 1a), which is likely due to the depleted nature of N Slave spinel peridotite (Kopylova and Russell 2000). Fe^{3+} concentrations in garnet are correlated with temperature (Fig. 1b), similar to observations already in

Table 2 Garnet $Fe^{3+}/\Sigma Fe$, pressure, temperature and relative oxygen fugacities for garnet-bearing equilibria in Slave peridotites and pyroxenites

Rock type	Sample no.	$Fe^{3+}/\Sigma Fe$ in grt	T (°C)		P (kbar)		ΔfO_2 (FMQ)	
			FB–MG[a]	BK–AlBK[b]	FB–MG[a]	BK–AlBK[b]	GW–FB–MG[c]	GW–BK–AlBK[d]
N Slave perodotite and pyroxenite xenoliths								
Low-T spinel–garnet peridotite								
Coarse	10-12a	0.030 (15)	700	792	27.6	30.3	−1.5	−1.8
Coarse	21-1	0.033 (20)	786	811	31.3	30.8	−2.0	−1.9
Coarse	26-11	0.061 (20)	851	944	39.3	42.7	−1.9	−2.1
Coarse	22-5	0.061 (20)	892	951	42.6	42.9	−2.3	−2.2
Coarse	25-4	0.058 (15)	868	975	41.2	47.7	−2.1	−2.6
Low-T garnet peridotite								
Coarse	25-9	0.026 (15)	781	842	35.3	36.6	−3.1	−3.1
Coarse	14-107	0.157 (20)	970	1,068	48.9	51.6	−1.9	−1.9
Coarse	40-11	0.060 (20)	1,048	1,104	55.2	52.1	−3.9	−3.4
Coarse	21-6	0.060 (15)	1,094	1,190	57.0	62.2	−3.9	−4.2
Coarse	21-4	0.054 (20)	1,019	1,097	51.7	55.2	−3.6	−3.8
Deformed	21-3	0.047 (15)	994	1,088	48.7	51.2	−3.6	−3.7
High-T garnet peridotite								
Deformed	22-7	0.085 (25)	1,121	1,187	57.7	53.4	−3.4	−2.9
Deformed	41-1	0.143 (30)	1,217	1,274	60.5	55.5	−3.0	−2.4
Deformed	8-1	0.068 (20)	1,228	1,282	61.4	56.4	−4.1	−3.5
Deformed	14-78	0.050 (15)	1,236	1,300	62.0	59.0	−4.6	−4.2
Deformed	40-38	0.134 (25)	1,228	1,286	62.2	49.5	−3.2	−2.0
Deformed, fertile	23-5	0.107 (20)	1,193	1,262	58.5	59.2	−3.2	−3.2
Garnet pyroxenite and megacrysts								
Megacrystalline pyroxenite	9-10	0.096 (15)	1,126	1,214	56.8	62.9	−3.2	−3.5
Megacrystalline pyroxenite	14-124	0.087 (20)	1,121	1,230	56.9	64.2	−3.4	−3.8
Megacrysts	41-3	0.123 (20)	1,213	1,281	59.1	60.0	−3.2	−3.1
SE Slave peridotite xenoliths								
Low-T garnet peridotite								
Coarse	32-2	0.099 (20)	1,047	1,178	59.1	68.3	−3.6	−4.1
Coarse	99-12	0.053 (15)		1,026[e]		56.5	−4.2	−4.2
Coarse	18-1	0.071 (20)	1,040	1,139	57.3	61.7	−3.6	−3.8
Coarse	38-2	0.037 (15)		971[e]		49.1	−3.9	−3.9
Deformed	11-5	0.100 (20)	1,113	1,255	64.8	64.8	−4.0	−3.6
Deformed	99-14C	0.078 (20)		1,027[e]		52.3	−3.1	−3.1
Deformed	38-1	0.060 (15)	1,024	1,122	57.3	62.3	−4.0	−4.2

[a]Based on the opx-cpx geothermometer of Finnerty and Boyd (1987) (FB) and the Al in opx (grt) geobarometer of MacGregor (1974) (MG)
[b]Based on the opx-cpx geothermometer of Brey and Köhler (1990) (BK) and the Al in opx (grt) geobarometer of Brey and Köhler (1990) (AlBK)
[c]Based on the grt-ol-opx oxybarometer of Gudmundsson and Wood (1995) (GW) combined with FB temperatures and MG pressures
[d]Based on the grt-ol-opx oxybarometer of Gudmundsson and Wood (1995) (GW) combined with BK temperatures and AlBK pressures
[e]Cpx is absent or altered in these samples; hence PT estimates are based on the ol-grt geothermometer of O'Neill and Wood (1979) and the Al in opx (grt) geobarometer of Brey and Köhler (1990)

Table 3 Spinel $Fe^{3+}/\Sigma Fe$, pressure, temperature and relative oxygen fugacities for spinel-bearing equilibria in N Slave peridotites

Rock type	Sample no.	$Fe^{3+}/\Sigma Fe$ in spl	T (°C)			P (kbar)			ΔfO_2 (FMQ)		
			OW–gth[a]	FB–MG[b]	BK–AIBK[c]	OW–gth[a]	FB–MG[b]	BK–AIBK[c]	W–OW–gth[d]	B–OW–gth[e]	xOW–OW–gth[f]
Low-T spinel peridotite											
Coarse	8-7	0.075 (20)	734	535	683	30	17[g]	25[h]	−1.3	−1.9	−3.1
Coarse	9-12	0.093 (20)	763			30			−0.9	−1.5	−2.8
Coarse	11-18	0.051 (20)	715			30			−1.8	−2.5	−3.9
Coarse	44-12	0.056 (20)	685	647	771	30	30[g]	30[h]	−1.8	−2.4	−3.6
Low-T spinel-garnet peridotite											
Coarse	10-12a	0.184 (30)	782	700	792	35	27.6	30.3	0.4	0.0	−1.4
Coarse	21-1	0.196 (30)	846	786	811	40	31.3	30.8	0.4	0.0	−1.6
Coarse	26-11	0.231 (30)	845	851	944	40	39.3	42.7	0.6	0.2	−1.2

[a]Based on the ol-spl geothermometer of O'Neill and Wall (1987) (OW) and the intersection of OW temperatures with the N Slave geotherm
[b]Based on the opx-cpx geothermometer of Finnerty and Boyd (1987) (FB) and the Al in opx (grt) geobarometer of MacGregor (1974) (MG)
[c]Based on the opx-cpx geothermometer of Brey and Köhler (1990) (BK) and the Al in opx (grt) geobarometer of Brey and Köhler (1990) (AlBK)
[d]Based on the spl-ol-opx oxybarometer of Wood (1990) (W) combined with OW temperatures and geotherm pressures
[e]Based on the spl-ol-opx oxybarometer of Ballhaus et al. (1991) combined with OW temperatures and geotherm pressures
[f]Based on the spl-ol-opx oxybarometer of O'Neill and Wall (1987), updated by H.S.C. O'Neill (personal communication) (xOW) combined with OW temperatures and geotherm pressures
[g]Pressure was determined by projecting the FB univariant P–T line onto the N Slave geotherm
[h]Pressure was determined by projecting the BK univariant P–T line onto the N Slave geotherm

the literature (indicated by shaded area in Fig. 1b) (Luth et al. 1990; Canil and O'Neill 1996; Woodland and Peltonen 1999; Woodland and Koch 2003), which may be related to both a temperature-dependent partitioning of Fe^{3+} between minerals (Canil and O'Neill 1996) and an increase in the bulk Fe_2O_3 concentration with depth (Woodland and Peltonen 1999).

Garnet thermobarometry and oxybarometry

For the garnet peridotite assemblage we used two sets of equilibrium P–Ts that were found to be consistent with the mineralogy and petrology of the Slave peridotite. Both sets of P–T estimates satisfy independent petrological constraints, e.g., potentially diamondiferous samples plot in the diamond stability field, and spinel–garnet peridotites plot around the spinel–garnet transformation curve (Kopylova et al. 1999; Kopylova and Caro 2004). These are temperature and pressure estimates made by (1) the two-pyroxene geothermometer of Brey and Köhler (1990) (BK) combined with the Al-in-opx geobarometer of Brey and Köhler (1990) (AlBK); and (2) the two-pyroxene geothermometer of Finnerty and Boyd (1987) (FB) combined with the Al-in-opx geobarometer of MacGregor (1974) (MG); both are listed in Table 2. The BK temperatures are approximately 50–100°C higher than the FB temperatures, while the two pressure estimates show no systematic variation and their difference is generally < 5 kbar.

We calculated oxygen fugacity using the garnet-olivine-orthopyroxene oxybarometer of Gudmundsson and Wood (1995) (GW), incorporating the typographical correction noted by Woodland and Peltonen (1999). Oxygen fugacities were calculated relative to the FMQ buffer ($\Delta\log fO_2$ [FMQ]) based on $Fe^{3+}/\Sigma Fe$ Mössbauer determinations in garnet. We calculated relative oxygen fugacities using both sets of P–T estimates (FB–MG and BK–AlBK) and found no systematic variation between the two results (Table 2). For a comparison of relative uncertainty contributions, the typical error of 0.02 in garnet $Fe^{3+}/\Sigma Fe$ for these samples produces a variation in $\Delta\log fO_2$ of 0.4–0.5 log-bar units, while a temperature uncertainty of 100°C produces a variation in $\Delta\log fO_2$ of only 0.1 log-bar units. Pressure uncertainty has a slightly larger effect than temperature, where a 3-kbar variation in pressure produces a $\Delta\log fO_2$ variation of 0.3–0.4 log-bar units.

Spinel thermobarometry and oxybarometry

It is more difficult to assess equilibrium conditions for the spinel–orthopyroxene–olivine paragenesis. As a first approach (1), we calculated temperatures using the olivine-spinel thermometer of O'Neill and Wall (1987) (OW) at pressures consistent with the N Slave geotherm (Kopylova et al. 1999). Using this method all spinel peridotites were determined to have equilibrated at

30 kb, and the spinel–garnet peridotites at 35–40 kb (Table 3), which is consistent with the estimated location of the spinel–garnet transformation curve for the N Slave peridotites (Kopylova et al. 1999). To check for consistency in temperature, we compared the OW temperatures with those determined from two-pyroxene thermometry (FB or BK), again assuming equilibration on the N Slave geotherm, and found that the BK temperatures were generally higher by 20–100°C, while the FB temperatures were lower by 0–80°C. As a second approach (2) we calculated temperature using a two-pyroxene thermometer for lherzolites (FB or BK) at pressures estimated based on the Al-in-opx geobarometer (MG or BK) for garnet-bearing samples, and on the intersection of temperatures with the N Slave geotherm for garnet-free rocks (Table 3). The extrapolation of the N Slave geotherm to garnet-free peridotite assumes a common steady-state thermal regime for the garnet-bearing and the garnet-free mantle, but this is supported by analysis of the surface heat flow and the surface heat generation on the N Slave craton (Russell and Kopylova 1999). As seen in Table 3, however, the uncertainty in pressure is larger than for the garnet-bearing assemblage.

We calculated relative oxygen fugacity using three different formulations of the spinel–olivine–orthopyroxene oxybarometer: (1) Ballhaus et al. (1991) (B); (2) O'Neill and Wall (1987) updated by H.S.C. O'Neill (personal communication) [1] (xOW) and (3) Wood (1990) (W). Oxygen fugacities were calculated relative to the FMQ buffer ($\Delta\log f\mathrm{O_2}$ [FMQ]) based on $\mathrm{Fe^{3+}}/\Sigma\mathrm{Fe}$ Mössbauer determinations in spinel. To simplify comparison between different oxybarometers, we based all calculations on PT estimates from the OW geothermometer intersected with the N Slave geotherm. The effect of uncertainties in pressure, temperature and composition on $\Delta\log f\mathrm{O_2}$ is similar for all three oxybarometers, where a temperature uncertainty of 200°C produces a variation in $\Delta\log f\mathrm{O_2}$ of 0.2 log-bar units, and a pressure uncertainty of 10 kbar produces a variation in $\Delta\log f_2$ of 0.3–0.4 log-bar units. For comparison, the typical error of 0.02 in spinel $\mathrm{Fe^{3+}}/\Sigma\mathrm{Fe}$ for these samples produces a variation in $\Delta\log f\mathrm{O_2}$ of 0.2 log-bar units.

The three formulations of the spinel–olivine–orthopyroxene oxybarometer give significantly different estimates (up to two log-bar units different) for relative oxygen fugacity in spinel-bearing peridotites (Table 3). This contrasts with experiments by Wood (1990, 1991) who found agreement using the same three formulations to within one log-bar unit. Also, Gudmundsson and Wood (1995) reported an experiment with co-existing olivine, orthopyroxene, spinel and garnet, where $\mathrm{Fe^{3+}}/\Sigma\mathrm{Fe}$ could be determined for the latter two phases. We applied the three spinel oxybarometer formulations to their reported data, and found agreement of all $\Delta\log f\mathrm{O_2}$ values to within 0.5 log-bar units of the value determined from the garnet-olivine-orthopyroxene oxybarometer of Gudmundsson and Wood (1995). So why should samples from the Slave mantle yield such widely differing $\Delta\log f\mathrm{O_2}$ values compared to these experiments? The answer probably lies in the vastly different conditions and compositions between the experiments and the Slave mantle samples, including in temperature (1,200 vs. 600–1,000°C), redox conditions (near FMQ vs. at least two log-bar units below) and spinel $\mathrm{Cr}/(\mathrm{Cr}+\mathrm{Al})$ composition (0–0.6 vs. 0.7–0.9). Indeed, Ballhaus et al. (1991) noted that application of the spinel oxybarometer could lead to problems in the garnet lherzolite and diamond stability fields arising from nonstoichiometry or $\mathrm{Cr^{2+}}$ substitution in spinel. In addition, they advised caution at lower temperatures due to the effects of cation ordering. These uncertainties question the reliability of all spinel oxybarometer formulations for samples from the cratonic mantle (low-temperature, highly reducing, high Cr concentrations in spinel).

In the absence of experimental calibrations under the appropriate conditions, we have therefore evaluated spinel oxybarometer results based on independent information regarding the assemblage. There is strong petrographical and petrological evidence that spinel in the N Slave spinel–garnet peridotite is equilibrated with garnet and other peridotite minerals:

1. Spinel is in textural equilibrium with the peridotitic assemblage. The crystals are large, anhedral and interstitial, typical of primary peridotitic spinel and uncharacteristic of secondary euhedral fine-grained spinel after garnet or serpentinized olivine.
2. The garnet composition and chemical correlation trends between elements in garnet depend on the presence or absence of spinel in the paragenesis as summarised in Kopylova et al. (2000).
3. Compositions of olivine, orthopyroxene and clinopyroxene in spinel-bearing garnet peridotite are systematically different from those in spinel-free garnet peridotite (Kopylova et al. 1999).
4. Temperatures calculated using the Ni concentration in garnet thermometer are lower in spinel-bearing peridotite than in spinel-free peridotite (Kopylova et al. 1999).
5. Two-pyroxene and olivine-garnet temperatures computed for spinel-bearing garnet peridotite are systematically lower then those for spinel-free garnet peridotite (Kopylova et al. 1999).
6. Equilibrium pressures and temperatures for spinel–garnet peridotite (Kopylova et al. 1999) are consistent with the experimentally modelled transition from the spinel to garnet peridotite facies for a rock of a given olivine and spinel composition (O'Neill 1981). The equilibrium between spinel and garnet in the peridotite assemblage implies that any estimate of

[1] The updated formulation incorporates a revised $\mathrm{SiO_2}$ activity based on the reaction $\mathrm{Mg_2SiO_4}+\mathrm{SiO_2}=\mathrm{Mg_2Si_2O_6}$ calculated from thermodynamic data of Holland and Powell (1998), which results in a $\Delta\log f\mathrm{O_2}$ increase of approximately 0.5 log-bar units for all of our samples compared to the original formulation.

relative oxygen fugacity involving spinel should be identical to that involving garnet, which suggests that the lowest set of $\Delta\log fO_2$ estimates in Table 3 is the most appropriate. We have therefore adopted the O'Neill and Wall (1987) estimates from Table 3 for the discussion below, but we emphasise that it does not imply a general endorsement of the formulation over the others, but simply indicates that the formulation reproduces the oxygen fugacity most closely for these particular conditions.

Whole rock concentrations of Fe^{3+} and V

Spinel Fe^{3+} concentrations are significantly different for spinel peridotite compared to spinel–garnet peridotite. We examined how these concentrations relate to the bulk chemistry of the rocks, particularly bulk Fe_2O_3 and the abundance of V which also records oxygen fugacity (Canil 2002 and references therein).

The bulk Fe_2O_3 concentration is lower in spinel peridotite than in spinel–garnet peridotite or low-T and high-T garnet peridotite (Table 4). However only a minor portion of Fe^{3+} resides in primary peridotitic minerals (Canil et al. 1994). We supplemented whole rock Fe_2O_3 abundance determined by wet chemistry by calculation of total Fe_2O_3 abundance in primary minerals based on the Fe^{3+} content of individual minerals, their modal abundances and total Fe concentrations (O'Neill et al. 1993; Canil et al. 1994).

Modal abundances and bulk compositions were available from the N Slave dataset of Kopylova and Russell (2000). We used the bulk chemical data averaged for each rock type, $Fe^{3+}/\Sigma Fe$ values for spinel and garnet from Mössbauer spectroscopy, $Fe^{3+}/\Sigma Fe$ values for clinopyroxene based on the olivine-orthopyroxene-clinopyroxene oxybarometer (Luth and Canil 1993) (spinel facies) or garnet-clinopyroxene Fe^{3+} partitioning (Canil and O'Neill 1996) (garnet facies), and $Fe^{3+}/\Sigma Fe$ values for orthopyroxene based on orthopyroxene-clinopyroxene Fe^{3+} partitioning in both the spinel and garnet facies (Canil and O'Neill 1996). Following the observations of O'Neill et al. (1993), Canil et al. (1994) and our own unpublished data for mantle olivines, we assumed $Fe^{3+}/\Sigma Fe$ to be zero in olivine for all samples.

The calculated total Fe_2O_3 abundances averaged for each rock type are listed in Table 4, along with bulk chemical data. Spinel peridotite shows a greater chemical depletion than spinel–garnet peridotite as inferred from higher MgO and Mg-numbers of bulk compositions and minerals as well as lower bulk FeO_{total} (Kopylova and Russell 2000). The lower total Fe_2O_3 in

Table 4 Bulk and mineral compositions, mineral modes and estimated Fe_2O_3 residing in primary minerals in N Slave peridotite

	Spinel peridotite	Spinel–garnet peridotite	Low-T garnet peridotite	High-T garnet peridotite	Fertile garnet peridotite (sample 23-5)
Bulk chemical analysis[a]					
Number of samples included in average[b]	7	5	4	6	1
Mg-number, bulk rock	0.928 (4)	0.919 (5)	0.908 (2)	0.909 (4)	0.896
MgO in bulk rock (wt%)	45.6 (12)	43.6 (15)	43.1 (16)	44.6 (8)	39.1
Fe_2O_3 in bulk rock (wt%)[c]	1.0 (2)	1.3 (4)	1.8 (4)	1.7 (1)	1.2
FeO_{Total} in bulk rock (wt%)	6.3 (3)	6.9 (2)	7.7 (3)	8.0 (5)	8.1
CaO in bulk rock (wt%)	0.5 (2)	0.9 (2)	1.3 (4)	0.7 (4)	2.1
Al_2O_3 in bulk rock (wt%)	0.8 (4)	1.2 (3)	1.1 (6)	0.9 (2)	3.4
V in bulk rock (ppm)	24 (4)	33 (5)	46 (14)	30 (9)	70
Modal olivine (vol%)	74 (9)	69 (7)	75 (7)	80 (3)	60
Modal opx (vol%)	23 (9)	23 (5)	14 (5)	15 (3)	15
Modal cpx (vol%)	2.2 (9)	2.9 (9)	6.6 (22)	1.7 (9)	5.3
Modal spinel (vol%)	0.9 (10)	0.5 (3)			0.0
Modal garnet (vol%)		4.6 (20)	4.0 (28)	4.0 (12)	19
Mineral analysis					
Number of samples included in average[d]	4	5	6	6	1
$Fe^{3+}/\Sigma Fe$ in spinel	0.07 (2)	0.20 (2)			
$Fe^{3+}/\Sigma Fe$ in garnet		0.05 (2)	0.07 (5)	0.10 (4)	0.11
Measured Fe_2O_3 in spl (wt%)	1.2 (4)	5.2 (6)			
Measured Fe_2O_3 in gt (wt%)		0.5 (2)	0.6 (4)	0.8 (3)	1.0
Estimated Fe_2O_3 in opx (wt%)[e]	0.0–0.1	0.3–0.4	0.3–0.6	0.3–0.6	0.59
Estimated Fe_2O_3 in cpx (wt%)[f]	0.1–0.2	0.5–0.6	0.6–0.8	0.8–1.0	1.02
Total Fe_2O_3 in primary minerals (wt%)[g]	0.03 (2)	0.14 (2)	0.13 (3)	0.11 (3)	0.33
Average $\Delta\log fO_2$ (FMQ)[h]	−3.4 (5)	−2.1 (3)	−3.3 (8)	−3.0 (9)	−3.2

[a]Data from Kopylova and Russell (2000) (Table 1 in their background data set)
[b]Averaged according to rock type for all samples with LOI < 4wt%; numbers in parentheses indicate standard deviations for the average values
[c]According to volumetric measurements
[d]Data averaged according to rock type from Tables 1 and 2 and electron microprobe analysis
[e]Based on opx-cpx Fe^{3+} partitioning (Canil and O'Neill 1996)
[f]Based on ol-opx-cpx oxybarometer for spinel assemblages (Luth and Canil 1993) and grt-cpx Fe^{3+} partitioning for garnet assemblages (Canil and O'Neill 1996)
[g]Calculated using the method described by O'Neill et al. (1993)
[h]Calculated using modified O'Neill and Wall (1987) oxybarometer for spinel peridotite and Gudmundsson and Wood (1995) oxybarometer for garnet peridotite

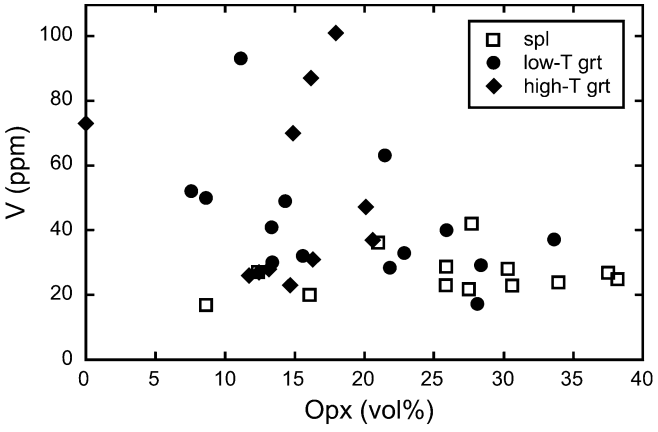

Fig. 2 Variation of V (ppm) with modal orthopyroxene (vol%) for N Slave peridotite. Whole rock V contents were analysed using XRF (Table 1 in EPSL Online Background Dataset, Kopylova and Russell 2000), while orthopyroxene modes were determined by image analysis and recalculation of bulk chemical analyses as described in Kopylova and Russell (2000)

spinel peridotite translates to an even greater reduction of Fe_2O_3 concentration in spinel, because Fe^{3+} is preferentially concentrated in that phase. Hence depletion results in more reducing conditions, where spinel peridotite shows $\Delta\log fO_2$ (FMQ) values more than one log-bar unit lower than for spinel–garnet peridotite (Table 3).

Spinel peridotite has lower concentrations of V (Table 4 and Fig. 2), but they cannot be taken as evidence for more oxidising conditions during melting in the Archean as proposed by Canil (2002). The low concentrations of bulk V in N Slave peridotite are often found in orthopyroxene-rich peridotite (Fig. 2), but the modes of orthopyroxene in these rocks are too high for simple melt residues (Kopylova and Russell 2000). The peridotite, therefore, cannot be generated by melt depletion, and the whole rock V concentrations, if modelled on such a premise (Canil 2002) leads to erroneous results (Lee et al. 2003).

Oxygen fugacity of cratonic peridotite

The final $\Delta\log fO_2$ estimates for spinel-bearing rocks from the Slave mantle calculated using the modified O'Neill and Wall (1987) spinel-orthopyroxene-olivine oxybarometer are plotted as a function of depth in Fig. 3a, and as expected from the significantly different $Fe^{3+}/\Sigma\ Fe_{spinel}$ ratios in spinel–garnet and spinel peridotites, spinel-garnet peridotite shows equilibration at higher $\Delta\log fO_2$ than garnet-free spinel peridotite (Fig. 3a). This conclusion is independent of both

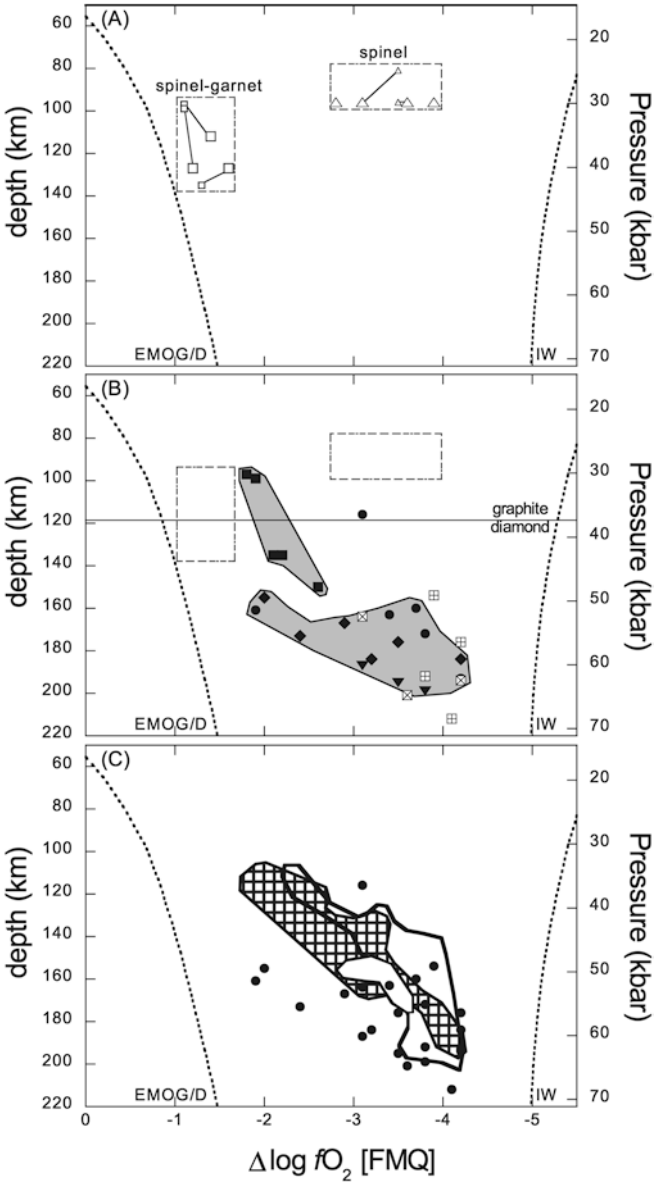

Fig. 3a–c Oxygen fugacity (relative to FMQ) of spinel and garnet peridotites and pyroxenites as a function of depth. **a** Relative oxygen fugacities estimated using the spinel-orthopyroxene-olivine oxybarometer (modified formulation of O'Neill and Wall 1987) for PT estimates based on (1) the OW thermometer and the projection onto the N Slave geotherm (*large symbols*) and (2) the BK–AlBK thermobarometer (*small symbols*). Estimates of $\Delta\log fO_2$ (FMQ) for the same samples using different PT estimates are connected by tie-lines. **b** Relative oxygen fugacities estimated using the garnet-orthopyroxene-olivine oxygen oxybarometer (Gudmundsson and Wood 1995) (GW) for PT estimates based on the AK–AlBK thermobarometer. Symbols are the same as for Fig. 1. Outlined P-$\Delta\log fO_2$ fields for spinel and spinel–garnet peridotite from spinel-based oxybarometry are transferred from Fig. 3a, and the *shaded fields* highlight the trends for N Slave spinel–garnet peridotite and N Slave garnet peridotite. The graphite-diamond equilibrium (Berman and Simon 1955) is based on the N Slave geotherm (Kopylova et al. 1999). **c** Relative oxygen fugacities estimated using the GW oxybarometer for all garnet-bearing rocks from the present work (*solid circles*) compared to values from the literature: large bold outlined field (Lesotho xenoliths, Woodland and Koch 2003); hatched field (South Africa xenoliths, ibid.); small white field (Fennoscandian xenoliths, Woodland and Peltonen 1999 as corrected by A.B. Woodland, personal communication). Buffer curves were calculated based on the N Slave geotherm (Kopylova et al. 1999) from Eggler and Baker (1982) (EMOG/D) and Ballhaus et al. (1991) (IW)

oxybarometer and thermobarometer choice. To illustrate the variation in $\Delta\log f\mathrm{O}_2$ for different thermobarometer solutions, we plotted two different estimates for each sample in Fig. 3a: (1) based on BK temperatures and AlBK pressures; and (2) based on OW temperatures projected onto the N Slave geotherm. Different thermobarometric estimates for each sample are joined by a line, and illustrate that despite a large uncertainty in pressure (up to 9 kbar), $\Delta\log f\mathrm{O}_2$ estimates for the same sample vary by <0.5 log-bar units. Therefore spinel–garnet peridotite equilibrated at more oxidising conditions than garnet-free spinel peridotite, irrespective of their estimated depth of origin, and independent of which spinel oxybarometer is used for the calculation.

The final $\Delta\log f\mathrm{O}_2$ estimates for garnet-bearing rocks from the Slave mantle calculated using the Gudmundsson and Wood (1995) garnet-orthopyroxene-olivine oxybarometer are plotted as a function of depth in Fig. 3b. The $\Delta\log f\mathrm{O}_2$ estimates for spinel–garnet peridotites are close to those calculated for the same rocks using the spinel-based oxybarometer (reproduced as a dashed box in Fig. 3b to facilitate comparison), although as noted in the previous section, the $\Delta\log f\mathrm{O}_2$ values calculated using spinel-based oxybarometry for diamondiferous cratonic spinel–garnet peridotites probably overestimate relative oxygen fugacity.

Garnet peridotites show a general reduction in $\Delta\log f\mathrm{O}_2$ with depth, where $\Delta\log f\mathrm{O}_2$ values of garnet peridotites are lower than those for spinel–garnet peridotites (Fig. 3b). Superimposed on this general trend is a degree of scatter arising from anomalously high- or low-Fe^{3+} concentrations in garnet for some of the N Slave coarse garnet peridotites. Relative oxygen fugacities of N Slave high-T peridotite also vary, even for samples from the same depth, and show no obvious trend with depth. These variations reflect a larger chemical variance in mineral compositions of pyroxenes and garnet that is also recorded in the large scatter of the BK temperature estimates. The relative oxygen fugacities of N Slave pyroxenites and megacrysts are similar to values for the N Slave high-T peridotites. The trend in relative oxygen fugacities of spinel-free coarse and deformed peridotites from the SE Slave are essentially identical to those from the N Slave. Even though SE Slave peridotites were equilibrated on a lower geotherm (Kopylova and Caro 2004), there is no observable effect on relative oxygen fugacity.

The relative oxygen fugacity estimates of spinel and garnet-bearing peridotites from the Slave mantle are consistent with all redox constraints implied by the sample petrology. Firstly, they are more oxidising than the IW buffer, where Ni is expected to reside in olivine instead of precipitating as metal (O'Neill and Wall 1987). This $\Delta\log f\mathrm{O}_2$ constrains the minimum fugacity and is applicable to peridotite with Ni-bearing olivine. Secondly, all of our relative oxygen fugacity estimates are more reducing than EMOG/EMOD buffer curves at the corresponding pressures (Fig. 3b). This $f\mathrm{O}_2$ constrains the maximum fugacity of peridotites equilibrated in the diamond stability field (above 940°C; Kopylova et al. 2000) based on the known presence of harzburgitic diamond in the Jericho and 5034 pipes.

Woodland and Koch (2003) reported relative oxygen fugacities for garnet peridotites from the Kaapvaal craton extending to depths of nearly 220 km, supplementing previous Kaapvaal data of Luth et al. (1990) and Canil and O'Neill (1996) (recalculated by McCammon et al. 2001). Also, Woodland and Peltonen (1999) presented relative oxygen fugacity data for the mantle beneath the Fennoscandian Shield from spinel–garnet and garnet peridotites to a depth of approximately 170 km. This literature data, together with our estimates, define a broad array of $\Delta\log f\mathrm{O}_2$ (FMQ) decreasing from -2 to -4 log-bar units over depths of 110 to nearly 220 km (Fig. 3c).

The reduction in relative oxygen fugacity with depth appears to be generally continuous within the data scatter for all of the garnet-only peridotite datasets. We note that the "kink" in the redox-depth profile reported by Woodland and Koch (2003) arises through their addition of $\Delta\log f\mathrm{O}_2$ data from spinel oxybarometry to the depth profile (their samples Let 19, Let 23 and Liq 9). If these data are omitted and only data from garnet-based oxybarometry are plotted, the trend is relatively linear for all data. This highlights the difference in oxygen fugacity variation between spinel and garnet peridotite, and is discussed further below in the context of redox control within the mantle.

All datasets converge in the deepest region which is dominated by deformed, high-T peridotite samples pervasively altered by asthenospheric melts that show $\Delta\log f\mathrm{O}_2$ values only one log-bar unit greater than the iron-wüstite buffer. The observation of such reducing conditions at these depths supports the growing consensus that the asthenosphere is relatively reduced (Green et al. 1987; Wood et al. 1990; Ballhaus and Frost 1994; Wood et al. 1996), instead of oxidised with a reduced lithosphere floating on top (Haggerty and Tompkins 1983; Haggerty 1986; Haggerty 1999).

The reduced nature of cratonic peridotitic mantle is fully consistent with all mineralogical constraints on oxygen fugacity available for these rocks, including the absence of carbonate in mantle xenoliths. Experiments have demonstrated that carbonate is stable in the presence of MgSiO_3 (as orthopyroxene or silicate perovskite) to at least 26 GPa (Katsura and Ito 1990); yet it is diamond and graphite, not carbonate, that are found in mantle peridotites under cratons. The lack of carbonate in mantle xenoliths hence rules out conditions more oxidising than the EMOD buffer ($\sim$FMQ-1). The overall reduced affinity of upper mantle minerals hosted by diamond (reviewed in Navon 1999) supports this estimate. Existing data suggests that off-cratonic subcontinental mantle may be reduced to a similar degree as the cratonic mantle (Pearson et al. 1994). Graphite and moissanite have been found in the off-cratonic subcontinental mantle (Lutkov et al. 1988), where relative oxygen fugacities of FMQ-3 to FMQ-1 have been reported (O'Neill and Wall 1987).

Oxygen fugacity and chemical depletion of the mantle

A number of studies have reported a correlation between depletion and oxygen fugacity in spinel-bearing peridotite (e.g., Wood et al. 1990; Bryndzia and Wood 1990; Daniels and Gurney 1991; Kadik 1997), which has been attributed to the slightly incompatible behaviour of Fe^{3+} during partial melting (e.g., Bryndzia and Wood 1990). Recently, Lee et al. (2003) modelled the redox evolution of residues produced by progressive melt depletion for fractional melting in a system closed to O_2 exchange. If the combined O_2 content of the melts and solid residue remains constant, $\Delta\log fO_2$ (FMQ) of the residues steadily decreases by 1.5 log-bar units as melting proceeds from ~5 to ~25%. Even though $\Delta\log fO_2$ estimates are not available for high degrees of melting typical of cratonic peridotites (20–40%, Walter 1998), it is clear that a strong depletion (> 5%) leads to reduced residues.

A correlation between depletion and oxygen fugacity is also observed in the spinel-bearing peridotite data from the N Slave craton (Table 4). The higher bulk MgO content of depleted samples is negatively correlated with bulk Fe_2O_3 according to the trend reported by Canil et al. (1994) (Fig. 4a). The lower bulk Fe_2O_3 concentration and amount of Fe_2O_3 present in primary phases in spinel peridotite leads to a significantly lower relative oxygen fugacity compared to spinel–garnet peridotite (Fig. 4b). This trend is most evident for averaged whole rock values (grey regions in Fig. 4) and less evident for individual samples (data points in Fig. 3). The individual samples are the few for which both whole rock chemistry and Mössbauer analysis were performed, and were not originally chosen to be representative of all samples within the given facies.

For comparison, we can evaluate the change in relative oxygen fugacity expected in an isochemical mantle with constant Fe_2O_3 abundance across the spinel–garnet peridotite transition. The change in relative oxygen fugacity depends critically on the partitioning of Fe^{3+} between garnet and spinel (Ballhaus and Frost 1994). N Slave spinel–garnet peridotites show K_D^{gt-sp} values for Fe^{3+} of roughly 0.2, implying that most Fe^{3+} remains concentrated in spinel, even in the presence of garnet. The reaction between spinel peridotite and spinel-garnet peridotite should therefore be associated with essentially zero change in relative oxygen fugacity (Fig. 3b in Ballhaus and Frost 1994), making the contrast in relative oxygen fugacity between spinel and spinel–garnet peridotite in the N Slave mantle even more striking. There the transition between spinel and spinel–garnet peridotite is not isochemical, but shows a distinct chemical boundary due to a less depleted composition, and the increased abundance of Fe_2O_3 in spinel results in an increased relative oxygen fugacity in spinel–garnet peridotite.

A correlation between depletion and oxygen fugacity in the spinel peridotite facies is expected to be strong because compositional changes in the residue during partial melting do not work against the effect of depleted Fe_2O_3 concentrations in reducing oxygen fugacity: (1) the modal abundance of spinel, orthopyroxene and clinopyroxene decreases with increased degrees of partial melting, and since these phases contribute similar amounts to whole rock Fe_2O_3 abundance (O'Neill et al. 1993), the tendency to concentrate Fe^{3+} in spinel with increasing depletion is reduced, and (2) olivine and orthopyroxene are on opposite sides of the oxygen fugacity equilibrium:

$$2Fe^{2+}\underset{sp}{Fe_2^{3+}O_4} + 6\underset{opx}{FeSiO_3} = 6\underset{ol}{Fe_2SiO_4} + O_2 \qquad (1)$$

(e.g., Wood 1991); hence coupled compositional variations have less effect on oxygen fugacity. The correlation between depletion and oxygen fugacity, however, may be obscured in many spinel peridotite suites (e.g., Parkinson and Arculus 1999; Ionov and Wood 1992) which may represent mixtures of variously depleted residues from different protoliths.

The relation between depletion and oxygen fugacity may be different in the spinel-free garnet peridotite stability field. Fertile garnet peridotite samples have been reported from the N Slave mantle that show bulk chemical patterns distinct from both low-T and high-T garnet peridotite (Fig. 6 in Kopylova and Russell 2000), and are represented in our dataset by sample 23-5. The garnet $Fe^{3+}/\Sigma Fe$ value is similar to those for other high-temperature peridotites (Fig. 1b and Table 2), but the significantly higher modal abundance of garnet in fertile peridotite leads to a higher calculated total Fe_2O_3 abundance (Table 4 and Fig. 4a). While this higher abundance is consistent with a more fertile composition, it does not necessarily result in a higher oxygen fugacity due to other compositional changes in the system (Fig. 4c). For example, the higher iron concentrations of olivine and orthopyroxene in the more fertile assemblage increase the activities of fayalite and ferrosilite, which then decrease oxygen fugacity through the equilibrium for spinel-free garnet peridotite:

$$2\underset{gt}{Fe_3^{2+}Fe_2^{3+}Si_3O_{12}} = 4\,\underset{ol}{Fe_2SiO_4} + 2\,\underset{opx}{FeSiO_3} + O_2 \qquad (2)$$

(Gudmundsson and Wood 1995). An Mg-number shift from 0.92 to 0.90 in olivine, for example, decreases $\Delta\log fO_2$ (FMQ) for sample 23-5 by nearly one log-bar unit.

The pattern in the garnet peridotite facies that depletion does not necessarily translate to a more reduced residue may be relevant on a more global scale. Compositional changes in the residue during partial melting tend to cancel out effects due to depleted Fe_2O_3 concentrations (which would normally lead to decreased oxygen fugacity), because (1) the modal abundance of garnet (the dominant contribution to whole rock Fe_2O_3) decreases (Table 4, see also Walter 1998), hence concentrating Fe^{3+} in the remaining garnet (which increases

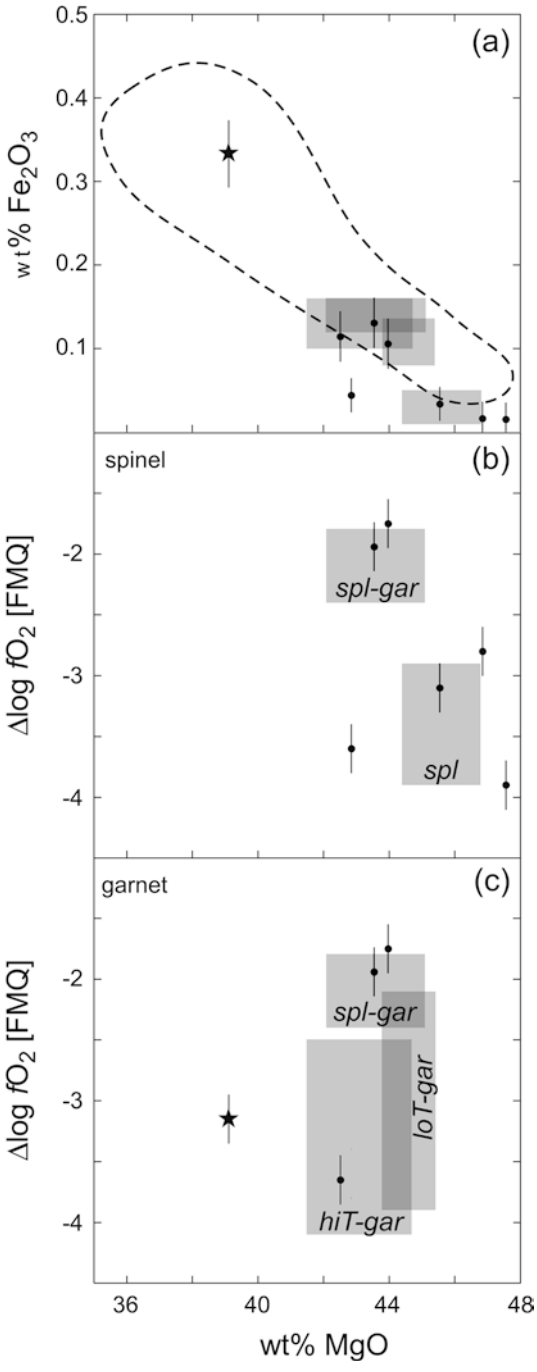

◀

Fig. 4 Effect of depletion (indicated by bulk MgO) on whole rock Fe_2O_3 content and relative oxygen fugacity. *Grey regions* are constructed from average values for N Slave peridotites plus one sigma standard deviations for each of the four peridotite facies (spinel, spinel–garnet, low-T garnet and high-T garnet) (Table 4). *Solid circles* indicate values for individual samples, while the star refers to fertile garnet peridotite (sample 23-5). Some of the individual analyses lie outside the grey regions because values deviate more than one standard deviation from the average. **a** Effect of depletion on whole rock Fe_2O_3 content. The N Slave samples follow the general trend reported by Canil et al. (1994) (dotted region). **b** Effect of depletion on relative fO_2 in the spinel-peridotite facies. The lower Fe_2O_3 contents in garnet-free spinel peridotite lead to lower relative fO_2. **c** Effect of depletion on relative f O2 in the garnet-peridotite facies. The effect of whole rock Fe_2O_3 content variations on relative fO_2 is small in garnet peridotite as discussed in the text

oxygen fugacity), and (2) olivine and orthopyroxene iron concentrations decrease, hence increasing oxygen fugacity. Pressure also plays a role, since the activity of the skiagite component in garnet is reduced with increasing pressure through the negative ΔV term for reaction 1 (e.g., Wood et al. 1990; Wood et al. 1996). This would reduce oxygen fugacity in deeper, more fertile assemblages compared to shallower, more depleted compositions. To compare the present results with other worldwide occurrences, we combined literature data of garnet peridotite whole rock analyses (Canil et al. 1994) with estimates of their relative oxygen fugacities (McCammon et al. 2001), and found a lack of correlation similar to that illustrated in Fig. 4c.

Control of oxygen fugacity in the cratonic peridotite mantle

Discussion regarding the control of oxygen fugacity in the mantle has been ongoing for more than two decades (see reviews by Arculus 1985; Wood et al. 1990; Luth 1999). If the mantle is assumed to be a closed system with no oxygen exchange with external sources, then oxygen fugacity is an intrinsic quantity that is completely determined by the bulk composition at a given pressure and temperature. The degree to which the system preserves this oxygen fugacity in the event of fluid infiltration or other influx of oxygen reflects the buffering capacity of the different equilibria, which depends in part on the concentration of oxidised species (e.g., Canil et al. 1994; Ballhaus 1995; Luth 1999). An appraisal of the relative buffering capacities of different equilibria (involving Fe, C, H or S) showed that no single equilibrium is considered to dominate overall (Canil et al. 1994), contributing to the generally accepted consensus that factors controlling oxygen fugacity likely vary in different parts of the mantle.

Within the cratonic mantle the control of oxygen fugacity is more unequivocal. Wood et al. (1990) argued that oxygen fugacity should decrease with depth within the garnet peridotite facies based on a highly negative ΔV term for the reaction, assuming that iron equilibria involving Fe^{3+} in garnet dominate over other equilibria in controlling oxygen fugacity. This was further quantified by Ballhaus (1995) and Wood et al. (1996), establishing the dominance of the pressure effect in reducing oxygen fugacity. These estimates were made before the first fO_2-depth profiles in the cratonic mantle were reported (Woodland and Peltonen 1999; Woodland and Koch 2003; this work), which emphasises the important evidence provided by these depth profiles of oxygen fugacity controlled primarily by garnet-based iron equilibria in the cratonic mantle.

Phase transitions involving iron-bearing phases should influence oxygen fugacity in a mantle where redox relations are dominated by iron. The depth variation of oxygen fugacity in the spinel–garnet perodotite facies should therefore be different compared to the garnet peridotite facies, partly due to the different ΔV terms for the redox reactions. The zero-pressure volume change for solids in the spinel–garnet peridotite reaction,

$$\underset{\text{gt}}{Fe_3^{2+}Fe_2^{3+}Si_3O_{12}} + \underset{\text{sp}}{Fe_3O_4} + 2\,\underset{\text{opx}}{FeSiO_3} = 5\,\underset{\text{ol}}{Fe_2SiO_4} + O_2, \quad (3)$$

is -17.8 cm^3 (relative to FMQ), which is significantly smaller than the corresponding value of -26.4 cm^3 for solids in the garnet peridotite reaction (Eq. 2) (based on data from Holland and Powell 1990 and Woodland and O'Neill 1993); hence we would expect a significantly greater reduction in oxygen fugacity with depth within the garnet peridotite facies. This is suggested by N Slave data that show a slope in $\Delta\log f\mathrm{O}_2$ (FMQ) versus pressure of 0.09–0.11 log-bar units/kbar for garnet peridotite, compared to only 0.04 log-bar units/kbar for spinel–garnet peridotite (Fig. 3b). This is further supported by the global dataset which shows a slope of roughly 0.09 log-bar units/kbar for garnet peridotite (Fig. 3b). In a similar way we can rule out a dominant control of oxygen fugacity by pyroxene-based iron equilibria (Luth and Canil 1993) because of the positive volume change relative to the FMQ buffer, implying that relative oxygen fugacity would increase with depth in a mantle dominated by pyroxene-based redox equilibria (Luth 1999).

The oxygen fugacity of the cratonic mantle is therefore related to its chemical and mineralogical boundaries, and is distinct in mantle domains of different composition. This rejects models where oxygen fugacity is controlled externally. However the oxygen fugacity measured from peridotites may not be representative of the redox state in all parts of the cratonic mantle, for example where eclogite is also present. The lower oxygen fugacities of depleted rocks could explain an observed strong preference of elemental carbon for cratonic harzburgite and eclogite. While average Archean mantle contains 85% lherzolite and 15% harzburgite, 85% of peridotitic diamonds are associated with depleted harzburgite (Grutter et al. 2003). Melting and depletion of harzburgites were likely to have occurred in the spinel-depth facies, even though harzburgites are now found at greater depths consistent with the presence of diamond. The shallow melting is suggested by extremely low concentrations of Al in cratonic peridotite, which cannot be achieved by melt extraction in the presence of garnet (Canil and Wei 1992; Kelemen et al. 1998; Canil 2002). Cratonic eclogite also represents the refractory residue produced by extraction of silicic trondjemite-tonalite-granodioritic magmas (Ireland et al. 1994; Barth et al. 2001). The lower oxygen fugacities of depleted rocks could also explain a geographical coincidence and excellent depth correlation between an ultra-depleted harzburgitic layer (Griffin et al. 1999) and a segment with low electromagnetic conductivity (Jones et al. 2001) of the Central Slave craton. The layers are mapped both geochemically and with a magnetotelluric survey down to ~100–150 km depth coincident with the graphite–diamond transformation. The higher abundance of graphite which has been invoked to explain the conductive shallow mantle of the central Slave (Jones et al. 2001) is therefore consistent with the reduced character of ultra-depleted harzburgites.

If the redox state of the mantle is controlled by Fe equilibria, then partial melts should be more oxidised than their spinel-bearing mantle sources. Indeed, MOR basalts have higher oxygen fugacity (up to three log units $\Delta\log f\mathrm{O}_2$) than their parent abyssal peridotites (Wood et al. 1990). A compilation of the most recent data on the redox state of arc mantle and arc magmas show a consistent difference of up to two to three log-units $\Delta\log f\mathrm{O}_2$ (Figs. 1 and 8 in Lee et al. 2003). Thus, the observed redox state of some magmas is consistently lower than that of the mantle protoliths and can constrain only the maximum $f\mathrm{O}_2$ of the mantle.

Concluding remarks

The following picture of the cratonic upper mantle has emerged as a result of this study. The subcontinental mantle is a mixture of domains with distinct compositions, and in the case of closed system behaviour, each domain can control its own oxygen fugacity that is predetermined by bulk composition, pressure and temperature. Predominant peridotitic segments interleave with eclogitic lenses that may have a different oxygen fugacity. Diamonds are stable in both lithologies, and carbonates are unstable in the cratonic peridotitic mantle because of the reduced conditions ($\Delta\log f\mathrm{O}_2$ [FMQ] = -1.5 to -4.5). The cratonic mantle is primarily buffered by the exchange of Fe^{2+} and Fe^{3+} between accessory spinel and garnet, and Fe^{2+} between olivine and pyroxenes; hence there is a change in oxygen fugacity with the disappearance of spinel with increasing depth in the peridotitic mantle. Relative oxygen fugacities of garnet-bearing cratonic peridotite decrease with depth in the range 80–210 km, reaching conditions one log-bar unit above the IW buffer. The reducing conditions within the cratonic mantle may be similar to those for off-cratonic mantle below continents.

Partial melting of the mantle redistributes Fe^{3+}, producing reduced residues and oxidised magmas. The availability of oxygen in the process of partial melting is not necessarily externally imposed, and thus melting cannot always be characterised by its "redox state". Segments of the mantle that experienced more extensive melting and hence extraction of Fe_2O_3 are more reduced, where the reduction is more pronounced in spinel peridotite than in garnet peridotite. Elemental carbon favours concentration in these depleted rocks, both

harzburgite and eclogite. Small amounts of material representative of this depleted reduced cratonic upper mantle are captured by diamonds as mineral inclusions. Subsequent partial melting of the mantle produces carbonate-rich magmas such as kimberlites, and while fluids associated with this magmatism are more oxidised than complementary reduced cratonic mantle, they can also be trapped in diamond.

Acknowledgements We thank J.K. Russell and D. Canil for discussions on various aspects of the study, and C. Sluggett for sample preparation. Various versions of the manuscript were improved through detailed reviews by A.B. Woodland and D. Canil. We are indebted to H. Cookenboo, Canamera Ltd, De Beers Canada and Mountain Province Ltd. for access to xenoliths from Slave kimberlites. Funding for this research was supported partly by an NSERC research grant to MGK (2000-current).

References

Amthauer G, Annersten H, Hafner SS (1976) The Mössbauer spectrum of ^{57}Fe in silicate garnets. Z Krist 143:14–55

Ballhaus C (1993) Redox states of lithospheric and asthenospheric upper mantle. Contrib Mineral Petrol 114:331–348

Ballhaus C (1995) Is the upper mantle metal-saturated? Earth Planet Sci Lett 132:75–86

Ballhaus C, Frost BR (1994) The generation of oxidized CO_2-bearing basaltic melts from reduced CH_4-bearing upper mantle sources. Geochim Cosmochim Acta 58:4931–4940

Ballhaus C, Berry RF, Green DH (1991) High pressure experimental calibration of the olivine-orthopyroxene-spinel oxygen barometer: implications for the oxidation state of the upper mantle. Contrib Mineral Petrol 107:27–40; corrected in Contrib Mineral Petrol (1991) 108:384–384 and Contrib Mineral Petrol (1994) 118:109

Barth M, Rudnick R, Horn I, McDonough W, Spicuzza M, Valley J, Haggerty S (2001) Geochemistry of xenolithic eclogites from West Africa, Part I: a link between low MgO eclogites and Archean crust formation. Geochim Cosmochim Acta 65:1499–1527

Berman R, Simon F (1955) On the graphite-diamond equilibrium. Z Elektrochem 59:333–338

Brey GP, Köhler T (1990) Geothermobarometry in four-phase lherzolites. II. New thermobarometers, and practical assessment of existing thermobarometers. J Petrol 31:1353–1378

Bryndzia LT, Wood BJ (1990) Oxygen thermobarometry of abyssal spinel peridotites: the redox state and C-O-H volatile composition of the Earth's sub-oceanic upper mantle. Am J Sci 290:1093–1116

Canil D (2002) Vanadium in peridotites, mantle redox and tectonic environments: Archean to present. Earth Planet Sci Lett 195:75–90

Canil D, O'Neill HSC (1996) Distribution of ferric iron in some upper-mantle assemblages. J Petrol 37:609–635

Canil D, Wei K (1992) Constraints on the origin of mantle-derived low Ca garnets. Contrib Mineral Petrol 109:421–430

Canil D, O'Neill HSC, Pearson DG, Rudnick RL, McDonough WF, Carswell DA (1994) Ferric iron in peridotites and mantle oxidation states. Earth Planet Sci Lett 123:205–220

Daniels LRM, Gurney JJ (1991) Oxygen fugacity constraints on the southern African lithosphere. Contrib Mineral Petrol 108:154–161

De Grave E, Van Alboom A (1991) Evaluation of ferrous and ferric Mössbauer fractions. Phys Chem Miner 18:337–342

Eggler DH, Baker DR (1982) Reduced volatiles in the system C-O-H: implications to mantle melting, fluid formation, and diamond genesis. In: Akimoto S, Manghnani MH (eds) High pressure research in geophysics. Center for Academic Publications Japan, Tokyo, pp 237–250

Finnerty AA, Boyd FR (1987) Thermobarometry for garnet peridotites: basis for the determination of thermal and compositional structure of the upper mantle. In: Nixon PH (ed) Mantle xenoliths. Wiley, Chichester, pp 381–402

Green DH, Falloon TJ, Taylor WR (1987) Mantle-derived magmas—roles of variable source peridotite and variable C-H-O fluid compositions. In: Mysen BO (ed) Magmatic processes and physiochemical principles, vol 1. Geochemical Society, USA, pp 139–154

Griffin WL, Doyle BJ, Ryan CG, Pearson NJ, O'Reilly SY, Natapov L, Kivi K, Kretschmar U, Ward J (1999) Lithosphere structure and mantle terrances: Slave craton, Canada. In: Gurney JJ, Gurney JL, Pascoe MD, Richardson SH (eds) The JB Dawson volume, proc VII international kimberlite conference. Red Roof Design, Cape Town, pp 299–306

Grutter H, Gurney JJ, Nowicki T (2003) Interpretation of kimberlite indicator mineral compositions: a key diamond exploration tool. In: "Diamonds", MDRU short course #37, 25–26 January 2003, Vancouver

Gudmundsson G, Wood BJ (1995) Experimental tests of garnet peridotite oxygen barometry. Contrib Mineral Petrol 119:56–67

Haggerty SE (1986) Diamond genesis in a multiply-constrained model. Nature 320:34–38

Haggerty SE (1999) A diamond trilogy: superplumes, supercontinents and supernovae. Science 285:851–860

Haggerty SE, Tompkins LA (1983) Redox state of Earth's upper mantle from kimberlitic ilmenites. Nature 303:295–300

Heaman LM, Kjarsgaard B, Creaser RA The timing of kimberlite magmatism and implications for diamond exploration: a global perspective. Lithos (in press)

Holland TJB, Powell R (1990) An enlarged and updated internally consistent thermodynamic dataset with uncertainties and correlations: the system K_2O-Na_2O-CaO-MgO-MnO-FeO-Fe_2O_3-Al_2O_3-TiO_2-SiO_2-C-H_2-O_2. J Metamorph Geol 8:89–124

Holland TJB, Powell R (1998) An internally consistent thermodynamic data set for phases of petrological interest. J Metamorph Geol 16:309–343

Ionov DA, Wood BJ (1992) The oxidation state of subcontinental mantle: oxygen thermobarometry of mantle xenoliths from central Asia. Contrib Mineral Petrol 111:179–193

Ireland TA, Rudnick RL, Spetsius Z (1994) Trace elements in diamond inclusions from eclogites reveal link to Archean granites. Earth Planet Sci Lett 128:199–213

Jones A, Ferguson I, Chave A, Evans R, McNeice G (2001) Electric lithosphere of the Slave craton. Geology 29:423–426

Kadik A (1997) Evolution of Earth's redox state during upwelling of carbon-bearing mantle. Phys Earth Planet Int 100:157–166

Katsura T, Ito E (1990) Melting and subsolidus phase-relations in the $MgSiO_3$-$MgCO_3$ system at high pressures—implications to evolution of the Earth's atmosphere. 99:110–117

Kelemen P, Hart S, Bernstein S (1998) Silica enrichment in the continental upper mantle via melt/rock reaction. Earth Planet Sci Lett 164:387–406

Kopylova MG, Caro G (2004) Mantle xenoliths from the southeastern Slave craton: Evidence for chemical zonation in a thick, cold lithosphere. J Petrol 45:1045–1067

Kopylova MG, Russell JK (2000) Chemical stratification of cratonic lithosphere: constraqints from the northern Slave craton, Canada. Earth Planet Sci Lett 181:71–87

Kopylova MG, Russell JK, Cookenboo H (1999) Petrology of peridotite and pyroxenite xenoliths from the Jericho kimberlite: implications for the thermal state of the mantle beneath the Slave craton, northern Canada. J Petrol 40:79–104

Kopylova MG, Russell JK, Stanley C, Cookenboo H (2000) Garnet from Cr- and Ca-saturated mantle: Implications for diamond exploration. J Geochem Explor 68:183–199

Lee CA, Brandon AD, Norman M (2003) Vanadium in peridotites as a proxy for paleo-fO_2 during partial melting: prospects, limitations, and implications. Geochim Cosmochim Acta 67:3045–3064

Li Z, Ping JY, Jin MZ, Liu ML (2002) Distribution of Fe^{2+} and Fe^{3+} and next-nearest neighbour effects in natural chromites: comparison between results of QSD and Lorentzian doublet analysis. Phys Chem Miner 29:485–494

Luth RW (1999) Carbon and carbonates in the mantle. In: Fei Y, Bertka CM, Mysen BO (eds) Mantle petrology: field observations and high-pressure experimentation: a tribute to Francis R (Joe) Boyd, vol 6. Geochemical Society, USA, pp 297–316

Luth RW, Canil D (1993) Ferric iron in mantle-derived pyroxenes and a new oxybarometer for the mantle. Contrib Mineral Petrol 113:236–248

Luth RW, Virgo D, Boyd FR, Wood BJ (1990) Ferric iron in mantle-derived garnets. Implications for thermobarometry and for the oxidation state of the mantle. Contrib Mineral Petrol 104:56–72

Lutkov VC, Sharapov NV, Gopfauf LM (1988) Petrochemical types of alkaline basalts from the South Tien-Shan (in Russian). Dokl Akad Nauk SSSR 303:1221–1225

MacGregor ID (1974) The system MgO-Al_2O_3-SiO_2: solubility of Al_2O_3 in enstatite for spinel and garnet peridotite compositions. Am Mineral 59:110–119

McCammon CA (1994) A Mössbauer milliprobe: psractical considerations. Hyper Inter 92:1235–1239

McCammon CA, Chaskar V, Richards GG (1991) A technique for spatially resolved Mössbauer spectroscopy applied to quenched metallurgical slags. Meas Sci Technol 2:657–662

McCammon CA, Griffin WL, Shee SH, O'Neill HSC (2001) Oxidation during metasomatism in ultramafic xenoliths from the Wesselton kimberlite, South Africa: implications for the survival of diamond. Contrib Mineral Petrol 141:287–296

Navon O (1999) Diamond formation in the Earth's mantle. In: Gurney JJ, Gurney JL, Pascoe MD, Richardson SH (eds) The PH Nixon volume, Proc VII international kimberlite conference. Red Roof Design, Cape Town, pp 584–604

O'Neill HSC (1981) The transition between spinel lherzolite and garnet lherzolite, and its use as a geobarometer. Contrib Mineral Petrol 77:185–194

O'Neill HSC, Wall VJ (1987) The olivine-orthopyroxene-spinel oxygen geobarometer, the nickel precipitation curve, and the oxygen fugacity of the Earth's upper mantle. J Petrol 28:1169–1191

O'Neill HSC, Wood BJ (1979) An experimental study of Fe–Mg partitioning between garnet and olivine and its calibration as a geothermometer. Contrib Mineral Petrol 70:59–70; corrected in Contrib Mineral Petrol (1980) 72:337

O'Neill HSC, Rubie DC, Canil D, Geiger CA, Ross CR II, Seifert F, Woodland AB (1993) Ferric iron in the upper mantle and in transition zone assemblages: implications for relative oxygen fugacities in the mantle. In: Takahashi T, Jeanloz R, Rubie DC (eds) Evolution of the earth and planets. Am Geophys Union, Washington, pp 73–88

Parkinson IJ, Arculus RJ (1999) The redox state of subduction zones: Insights from arc-peridotites. Chem Geol 160:409–423

Pearson DG, Boyd FR, Haggerty SE, Pasteris JD, Field SW, Nixon PH, Pokhilenko NP (1994) The characterization and origin of graphite in cratonic lithospheric mantle: a petrological carbon isotope and Raman spectroscopic study. Contrib Mineral Petrol 115:449–466

Russell JK, Kopylova MG (1999) A steady-state conductive geotherm for the north-central Slave, Canada: Inversion of petrological data for the Jericho kimberlite pipe. J Geophys Res 104:7089–7101

Walter MJ (1998) Melting of garnet peridotite and the origin of komatiite and depleted lithosphere. J Petrol 39:29–60

Wood BJ (1990) An experimental test of the spinel peridotite oxygen barometer. J Geophys Res 95:15845–15851

Wood BJ (1991) Oxygen barometry of spinel peridotites. In: Lindsley DH (ed) Oxide minerals: petrologic and magnetic significance. Miner Soc Am, Washington, pp 417–431

Wood BJ, Bryndzia LT, Johnson KE (1990) Mantle oxidation state and its relationship to tectonic environment and fluid speciation. Science 248:337–345

Wood BJ, Pawley A, Frost D (1996) Water and carbon in the earth's mantle. Phil Trans R Soc Lond A 354:1495–1511

Woodland AB, Koch M (2003) Variation in oxygen fugacity with depth in the upper mantle beneath the Kaapvaal craton, Southern Africa. Earth Planet Sci Lett 214:295–310

Woodland AB, O'Neill HSC (1993) Synthesis and stability of $Fe_3^{2+}Fe_2^{3+}Si_3O_{12}$ garnet and phase relations with $Fe_3Al_2Si_3O_{12}$- $Fe_3^{2+}Fe_2^{3+}Si_3O_{12}$ solutions. Am Mineral 78:1002–1015

Woodland AB, Peltonen P (1999) Ferric iron contents of garnet and clinopyroxene and estimated oxygen fugacities of peridotite xenoliths from the eastern Finland kimberlite province. In: Gurney JJ, Gurney JL, Pascoe MD, Richardson SH (eds) The PH Nixon volume, Proc VII international kimberlite conference. Red Roof Design, Cape Town, pp 904–911